Thermodynamic properties of the two-dimensional quantum Heisenberg ferromagnet and the effects of bond dilution

E. F. Talbot*
Department of Physics, University of California, Santa Barbara, California 93106
(Received 18 December 1985)

The energy, the specific heat, and the magnetic susceptibility of the bond-diluted $S=\frac{1}{2}$ Heisenberg ferromagnet on a two-dimensional square lattice are studied using a Monte Carlo sampling of the terms contributing to the partition function. The full lattice is studied in detail for sizes up to 20×20, and evidence is presented to suggest that the low-temperature correlation length behaves as $\xi\sim e^{\nu\beta J}$ with $\nu\sim1.91\pm0.06$. The temperature dependence of the susceptibility, however, is not quite a simple exponential in βJ. Knowledge of the correlation length and finite-size scaling allows the determination of the prefactor. Our conclusion is that the low-temperature susceptibility behaves as $T^{-1}e^{2\nu\beta J}$. Square lattices of size ranging from 6×6 to 12×12 are studied for k_BT/J ranging from 0.1 to 3 and for several values of the bond probability p. Not surprisingly, the most drastic thermodynamic behavior near the critical bond-percolation probability is the sharp increase in the low-temperature susceptibility for $p>p_c$. This corresponds to much larger correlation effects in the percolating lattice than below the percolation threshold. We also compare the thermodynamics at $p=p_c$ to the scaling theories of Lubensky and Stanley *et al.* which suggest that the correlations at the percolation threshold are predominantly one dimensional.

I. INTRODUCTION

It is known that the classical Heisenberg model does not order at any finite temperature in two dimensions.[1-3] Quantum fluctuations would make the two-dimensional (2D) quantum Heisenberg model even less likely to order than the classical system. Hence, nothing as drastic as a phase transition is expected to occur in the 2D quantum Heisenberg ferromagnet (HF). The quantum system is, however, not entirely devoid of interest as some real materials such as K_2CuF_4 seem to have very nearly the same magnetic interactions as the 2D $S=\frac{1}{2}$ HF.[4,5] There has been a good deal of theoretical work on bond-diluted lattices, particularly in the percolation limit,[6] and one of the main purposes of this article is to extend this work to the study of the thermodynamics of the bond-diluted $S=\frac{1}{2}$ 2D HF. Bond-diluted lattices are more amenable to various approximations such as the effective-medium approximation[7] than are the more physically realizable site-diluted lattices. Both quenched dilute systems are nonetheless expected to exhibit the same qualitative behavior, and studying the thermodynamic behavior of the bond-diluted system will give us insight into the behavior of the site-diluted system. The main difference between the two diluted lattices is in the percolation threshold probability p_c. On the 2D square lattice the threshold bond concentration[8] is $p_c=0.5$ while the threshold site concentration[9] in the site-diluted system is $p_c\simeq0.59$. It is to be noted that the site-diluted problem can be studied just as easily with the technique used in this paper as the bond-diluted problem.

Most of the theoretical work done on the quantum 2D HF can be classified in one of two broad categories: (1) high-temperature series expansions[10] and the associated Padé approximations,[11,12] or (2) spin-wave theory[13] and other Green's-function approximations.[14] The high-temperature series expansions are accurate but of limited range of validity. Some Green's-function approximations, such as that of Yamaji and Kondo,[14] appear to be valid over a much wider range of temperatures but these always involve some uncontrolled approximations. Furthermore, experiments are difficult to perform and analyze because of lattice contributions to the thermodynamics and the fact that the magnetic Hamiltonian is only approximately two dimensional.[4] A numerical experiment such as a Monte Calo calculation can provide us with new information and insight which can be used to check existing approximate theories and guide future analytic approaches. Here we begin with a review of various results which have already been obtained.

Defining the bond strength J by the Hamiltonian

$$\hat{H}=-2J\sum_{\langle ij\rangle}\mathbf{s}_i\cdot\mathbf{s}_j\ , \tag{1.1}$$

where the sum is over all nearest-neighbor pairs, the spin-wave theory described by Dalton and Wood[13] (DW) predicts a low-temperature susceptibility of the form

$$\chi_{\rm DW}\sim AN\frac{(g\mu_B)^2}{J}\exp(2\pi/\theta)\ , \tag{1.2}$$

where $\theta\equiv k_BT/J$ is a dimensionless temperature, μ_B is the Bohr magneton, and g is the Landé factor. The more sophisticated Green's-function approximation used by Yamaji and Kondo[14] (YK) predicts that the susceptibility varies as

$$\chi_{\rm YK}\sim A'N\frac{(g\mu_B)^2}{J\theta}\exp\left[\frac{\pi}{\theta}-\frac{\pi^2}{16}\theta\right]\ . \tag{1.3}$$

In contrast, the susceptibility for the classical HF on a square lattice goes as[2]

$$\chi_c \sim A'' \frac{N\mu^2}{J_c} \left[\frac{k_B T}{J_c} \right]^2 \exp \left[\frac{4\pi J_c}{k_B T} \right] , \tag{1.4}$$

where the classical coupling constant is defined by the Hamiltonian

$$H_c = -J_c \sum_{\langle ij \rangle} \mathbf{s}_i \cdot \mathbf{s}_j \tag{1.5}$$

and $|\mathbf{s}_i|^2 = 1$. One of the purposes of this paper is to study the low-temperature behavior of the susceptibility and so resolve the question posed by the differences between (1.2) and (1.3). To this end we have also studied the temperature dependence of the correlation length. Knowledge of the correlation length allows us to use finite-size scaling to help determine the factor multiplying the exponential in βJ ($\beta J \equiv 1/\theta$) in the expression for χ.

As mentioned above, one of the objects of this article is to study the low-temperature behaviors of the susceptibility and the correlation length for the full 2D square lattice. We also consider the bond-diluted $S = 1/2$ 2D HF for a whole range of bond probabilities p. It has been suggested by Stanley *et al.*[15] and by Lubensky[16] that, near the percolation threshold, the system is made up of nodes connected by one-dimensional links. As the spin correlations propagate one dimensionally, the one-dimensional correlation length $\xi_1(T)$ plays a very important role near p_c. Indeed, for a Heisenberg chain,[17,18] we have $\xi_1(T) \sim \theta^{-1}$ and the spin correlation length and the susceptibility at p_c behave as[16,19]

$$\begin{aligned} &\xi \sim [\xi_1(T)]^{\nu_T} \sim \theta^{-\nu_T} , \quad \theta \to 0 \\ &T\chi \sim [\xi_1(T)]^{\gamma_T} \sim \theta^{-\gamma_T} , \quad \theta \to 0 . \end{aligned} \tag{1.6}$$

From scaling arguments[15,16] and renormalization-group calculations[19,20] one can define a crossover exponent

$$\phi \equiv \nu_p / \nu_T = \gamma_p / \gamma_T , \tag{1.7}$$

where ν_p and γ_p are percolation critical indices[6] describing the divergences of the connectivity correlation length and the size of the clusters as $p \to p_c$. For $d = 2$, Ref. 6 gives $\nu_p = 1.33$ and $\gamma_p = 2.43$. Coniglio[20] predicts that $\phi = 1.43$ for the classical Heisenberg system in 2D. Hence the prediction is that the classical 2D HF at $p = p_c$ has the behavior

$$\begin{aligned} &\xi \sim \theta^{-0.93} , \quad \theta \to 0 \\ &T\chi \sim \theta^{-1.7} , \quad \theta \to 0 . \end{aligned} \tag{1.8}$$

Stinchcombe[19] used an approximate form of real-space renormalization to get $\phi = 1.13$ for the 2D $S = \frac{1}{2}$ HF. In this article we attempt to obtain ν_T and γ_T directly from (1.6) and hence estimate ϕ for the 2D $S = \frac{1}{2}$ HF.

Monte Carlo calculations of the thermodynamics of quantum systems are a relatively recent development. Most such calculations[21] involve a path integral over the imaginary time interval $\beta = (k_B T)^{-1}$. Even the stochastic quantization method proposed by Parisi and Wu,[22] while it is not a true Monte Carlo technique, involves such a path integral over imaginary time. These techniques map the d-dimensional quantum system onto a system of dimensionality $d+1$ where we are to integrate over the paths or "states" weighted by a classical action. Such path integrals are almost invariably factored into integrals over time slices, and the corresponding Monte Carlo algorithms[21] become quite complicated in higher dimensions. Furthermore, the finite size of the time slices $\Delta\tau = \beta/L$ introduces some errors which are to be minimized or at least estimated by using different values of L.

It has recently been pointed out by Lyklema[23] and Chakravarty and Stein[24] that a Monte Carlo technique suggested by Handscomb[25] in 1962 converges sufficiently quickly for the technique to be useful in the study of the thermodynamics of the $S = \frac{1}{2}$ HF. The simplest form of this technique is only valid for the isotropic $S = \frac{1}{2}$ Heisenberg model and it is only efficient for a ferromagnetic interaction. Generalizations of the methods which allow the study of the antiferromagnetic Heisenberg model and the XY and XXZ models have also been presented.[24,26] The technique is, in essence, a Monte Carlo sampling of the vacuum-vacuum diagrams contributing to the partition function. An important feature of this technique is that the implementation of the algorithm is basically independent of the dimensionality or which bonds are present or missing in the Hamiltonian. Indeed, the method is ideally suited to the study of quenched diluted Heisenberg systems or Hamiltonians including next-nearest-neighbor interactions. The site-diluted system is treated in the same way as the bond-diluted case, the only difference being the definition of the existing bonds. It is this method that we will use to study the thermodynamics of the bond-diluted $S = \frac{1}{2}$ 2D HF.

As our simulations deal exclusively with the ferromagnetic case [$J > 0$ in Eq. (1.1)], we shall limit our formulas to the case $J > 0$. For $S = \frac{1}{2}$, we have the operator identity

$$2\mathbf{s}_i \cdot \mathbf{s}_j = \hat{P}_{ij} - \tfrac{1}{2} , \tag{1.9}$$

where the transposition operator $\hat{P}_{ij}$ interchanges the spin states of sites i and j. The Hamiltonian may then be written as

$$\hat{H} = -J \sum_{i=1}^{N_b} \hat{P}_i + \tfrac{1}{2} J N_b , \tag{1.10}$$

where $\hat{P}_i$ is the transposition operator associated with the ith bond, and N_b is the total number of bonds in the lattice. As the constant energy term $JN_b/2$ only determines the zero of energy, it will be neglected in what follows. The Hamiltonian is then simply a sum of permutation operators. The partition function can be expanded in powers of βJ:

$$\begin{aligned} Z &= \mathrm{Tr} e^{-\beta \hat{H}} \\ &= \sum_{n=0}^{\infty} \sum_{C_n} \Pi(C_n) , \end{aligned} \tag{1.11}$$

where

$$\Pi(C_n)\equiv\frac{(\beta J)^n}{n!}\mathrm{Tr}(\hat{C}_n)\ , \tag{1.12}$$

and

$$\hat{C}_n\equiv\hat{P}_{i_1}\hat{P}_{i_2}\cdots\hat{P}_{i_n}\ , \tag{1.13}$$

and the sum over C_n is a sum over all possible ordered sequences $(i_1 i_2\cdots i_n)$. The expectation value of an operator $\hat{A}$ is given by

$$\langle\hat{A}\rangle=\frac{1}{Z}\mathrm{Tr}(e^{-\beta\hat{H}}\hat{A})\ . \tag{1.14}$$

If we again expand in powers of βJ, we have

$$\langle\hat{A}\rangle=\sum_{n=0}^{\infty}\sum_{C_n}\frac{\Pi(C_n)}{Z}\Omega_A(C_n)\ , \tag{1.15}$$

where

$$\Omega_A(C_n)\equiv\frac{\mathrm{Tr}(\hat{C}_n\hat{A})}{\mathrm{Tr}(\hat{C}_n)}\ . \tag{1.16}$$

Our Monte Carlo algorithm (described in detail in the Appendix) will constitute a random walk among the various sequences C_n, each weighted by the probability $\Pi(C_n)/Z$. $\Omega_A(C_n)$ is then a classical observable corresponding to the quantum observable $\hat{A}$. This sampling of the C_n is essentially equivalent to a sampling of the vacuum-vacuum diagrams contributing to the partition function.[24] We may also consider this Monte Carlo procedure as a high-temperature expansion which includes terms of arbitrary order in βJ. Indeed the simulation will automatically consider almost exclusively the dominant terms in the expansion of Z.

We note that the index i_k in the sequence C_n can have any value from 1 to N_b. This feature is unchanged if certain bonds are deleted from the Hamiltonian. Bond dilution, site dilution, or even the dimensionality only affects the bonds to be included in the Hamiltonian. Other Monte Carlo techniques for studying the quantum spin problem are not so easily modified to study diluted systems or systems of higher dimensionality.

The remainder of this article is organized as follows. In Sec. II we present the data for the full 2D square lattice with particular emphasis on the nature of the divergence of the low-temperature susceptibility. Section III deals with the bond-diluted Heisenberg system. We present data on the specific heat and the susceptibility for the bond probabilities $p=0.25$, 0.5, and 0.75 on lattices of size 12×12. We describe the p dependence of the susceptibility at a fixed temperature for various lattice sizes and we give results for the correlation length at $p=0.75$ and at the percolation threshold $p_c=0.5$. The Appendix describes the Monte Carlo algorithm in detail and gives a discussion of its performance.

II. THE 2D HEISENBERG FERROMAGNET: FULL LATTICE RESULTS

In this section we shall present and discuss our results for the full square lattice. We measured the energy, the specific heat, the susceptibility, and the correlation function $G(M/\sqrt{2})$ defined as

$$G(M/\sqrt{2})=\frac{4}{N}\sum_i\langle s_i^z s_{i+r}^z\rangle\ , \tag{2.1}$$

where $N=M^2$ is the number of sites in the lattice and r is the largest separation between two sites in an $M\times M$ lattice, i.e., $r=(M/2,M/2)$. This last measurement enables the determination of the correlation length by studying different size lattices. We studied lattices of size 4×4 up to 20×20. A typical run consisted of ten groups of 2000 observations. The statistical fluctuations between the observation groups then determined the approximate uncertainties in the observables. At high temperatures the correlation length $\xi(T)$ becomes very small and $\xi(T)\ll M/\sqrt{2}$ even for the small lattices $M=4$ and 6. To measure the small $G(M/\sqrt{2})$, for small or moderate N ($N\lesssim144$ sites) some high-temperature runs were as long as ten groups of 10 000 observations. [The discussion following Eq. (A2) in the Appendix describes the limitations on the measurement of the correlation function $\langle s_i^z s_j^z\rangle$.]

Figure 1 shows the energy per bond as a function of the temperature as measured using the expression (A7). For comparison we have also included in Fig. 1 the curve obtained from the high-temperature series expansion of Baker *et al.*[10] For simplicity we only show our results for the 6×6 and the 20×20 lattices. The high-temperature series starts to deviate from our Monte Carlo results at $\theta\lesssim2$ and becomes unphysical at $\theta\lesssim1.1$. Our Monte Carlo pro-

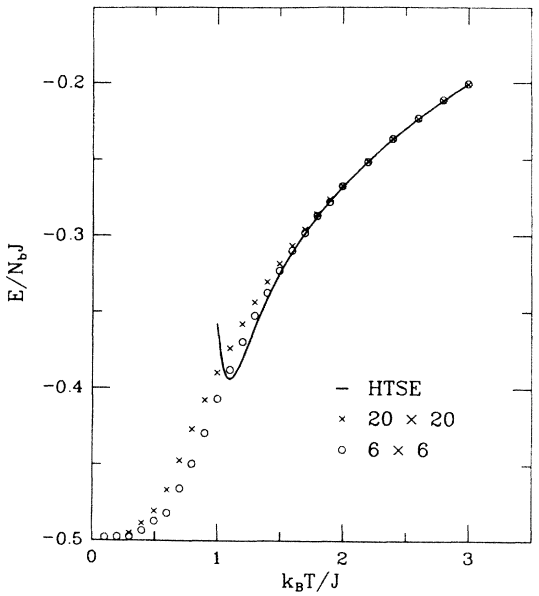

FIG. 1. The average energy per bond as a function of the temperature for two different lattice sizes. The solid line is the high-temperature series expansion (HTSE) of Baker, *et al.* (Ref. 10). The error bars are of the order of 0.002 for the 6×6 lattice results and of the order of 0.003 for the 20×20 lattice results.

cedure, however, gives essentially exact results albeit for finite-size lattices. As we will see below in our discussion of finite-size effects, it appears that the 20×20 lattice has the behavior of the thermodynamic limit for temperatures down to about $\theta=0.7$. The correlations in the 6×6 lattice saturate at low temperatures and consequently the energy is very flat for $\theta\lesssim0.3$.

In Fig. 2 we show the specific heat per bond as a function of the temperature for lattices of size 6×6, 10×10, and 20×20. We also compare these to the high-temperature series of Baker *et al.* As the lattice size grows, the specific-heat height stays roughly the same but shifts toward lower temperatures. The specific heat below $\theta=0.7$ is probably affected somewhat by the finite size of the lattice. One can nonetheless conclude that the specific-heat peak height is about $0.2k_B$ per bond and occurs at a temperature less than or equal to $0.7J$.

The most noticeable finite-size effect is probably the saturation of the low-temperature susceptibility. In Fig. 3 we present the susceptibility per site on a lattice of size $M\times M$ as a function of the temperature and for several values of M. In contrast to the high-temperature series for the specific heat we find that the high-temperature series for the susceptibility from Baker *et al.*[10] is quite good down to $\theta\lesssim0.7$. In the low-temperature limit, the susceptibility saturates at a value determined by the size of the system. It is a simple matter to derive this saturation level. Letting χ_0 denote the susceptibility of N independent spins, we have

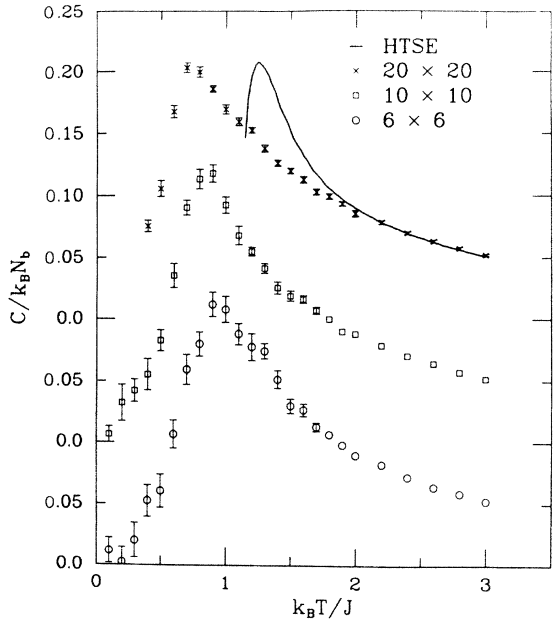

FIG. 2. The specific heat per bond as a function of the temperature for three different lattice sizes. The solid curve represents the high-temperature series expansion of Baker *et al.* (Ref. 10). We have translated the y axis for the three lattice sizes in order to separate the curves. The error bars not shown are smaller than the points drawn.

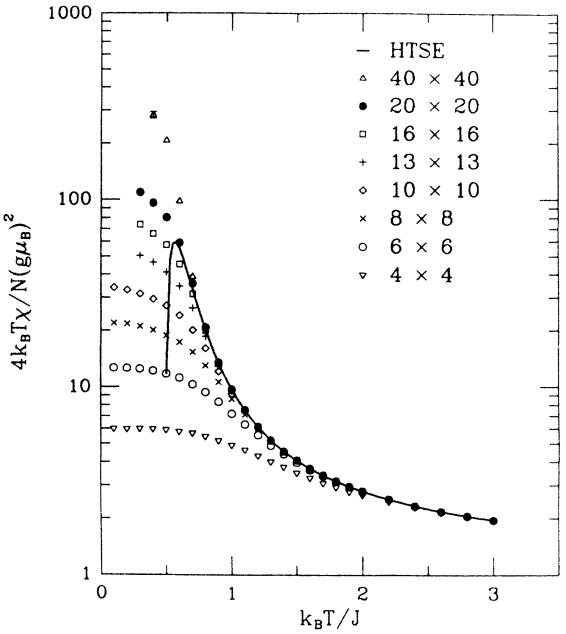

FIG. 3. The magnetic susceptibility per site $4k_BT\chi/N(g\mu_B)^2$ $(\equiv\chi'\chi_0)$ as a function of temperature for various lattice sizes. χ_0 is the susceptibility of N independent spins.

$$\chi_0=\frac{N(g\mu_B)^2}{4k_BT}\ , \tag{2.2}$$

and

$$\begin{aligned}\frac{\chi}{\chi_0}&=\frac{4}{N}\langle S^zS^z\rangle\\&=\frac{4}{N}\left[\frac{N}{4}+\sum_{\substack{i,j\\(i\neq j)}}\langle s_i^zs_j^z\rangle\right]\\&=\frac{4}{N}\left[\frac{N}{4}+\tfrac{1}{3}\sum_{\substack{i,j\\(i\neq j)}}\langle \mathbf{s}_i\cdot\mathbf{s}_j\rangle\right].\end{aligned} \tag{2.3}$$

Furthermore, the inner product $\mathbf{s}_i\cdot\mathbf{s}_j$ may be written as

$$\begin{aligned}\mathbf{s}_i\cdot\mathbf{s}_j&=\tfrac{1}{2}[(\mathbf{s}_i+\mathbf{s}_j)^2-\tfrac{3}{2}]\\&=\begin{cases}\frac{1}{4} & \text{in the triplet state}\\ -\frac{3}{4} & \text{in the singlet state}\ .\end{cases}\end{aligned} \tag{2.4}$$

As the temperature is lowered, this correlation takes on more and more a triplet character until at $T=0$ we have

$$\langle \mathbf{s}_i\cdot\mathbf{s}_j\rangle=\tfrac{1}{4} \tag{2.5}$$

for all $i\neq j$. Hence Eq. (2.3) becomes[27]

$$\begin{aligned}\lim_{T\to0}\frac{\chi}{\chi_0}&=\frac{4}{N}\left[\frac{N}{4}+\frac{N(N-1)}{3}\frac{1}{4}\right]\\&=\tfrac{1}{3}(N+2)\ .\end{aligned} \tag{2.6}$$

Figure 3 also includes the results of a short run (1000 observations) done on a 40×40 lattice. We see that saturation effects become important for the 20×20 lattice for $\theta\lesssim0.6$.

In an attempt to compare our results for the susceptibility with Dalton and Woods's spin-wave approximation[13] and Yamaji and Kondo's Green's-function approximation,[14] we have plotted in Fig. 4 the function

$$f(\zeta,\beta J)\equiv\ln\left[\frac{4J\chi}{N(g\mu_B)^2}\theta^{\zeta}\right]+\frac{3\zeta}{2} \tag{2.7}$$

versus βJ for $\zeta=-1$, 0, 1, and 2. The term $3\zeta/2$ in (2.7) simply separates the various curves. If the low-temperature susceptibility behaves as

$$\chi\sim T^{\zeta}\exp(\gamma\beta J)\ , \tag{2.8}$$

then $f(\zeta,\beta J)$ plotted as a function of βJ will be a straight line with slope γ in the limit $\beta J\to\infty$. Dalton and Wood [Eq. (1.2)] predict $(\zeta,\gamma)=(0,2\pi)$ while Yamaji and Kondo [Eq. (1.3)] predict $(\zeta,\gamma)=(-1,\pi)$. From the linearity at large βJ, Fig. 4 seems to indicate that ζ is near 1 or 2. If one fixes ζ at -1, 0, 1, or 2, one gets the corresponding values of γ given in Table I. Neither Dalton and Wood's prediction nor that of Yamaji and Kondo seem to fit the results. Of course it may be that our results, valid down to $\theta\simeq0.6$, do not represent the true low-temperature behavior. Nevertheless, the information in Fig. 4 and Table I is not to be ignored. In the following paragraphs, we will use finite-size scaling analysis and Table I to extract further information about ζ and γ.

TABLE I. Values of γ based on Eq. (3.8) assuming certain values of ζ. We implicitly assume that the trends of Fig. 4 continue toward $\beta J\to\infty$.

ζ	γ
-1	$\gtrsim3.9\ \pm0.1$
0	$\gtrsim4.5\ \pm0.1$
1	5.09 ± 0.07
2	5.78 ± 0.05

In order to get more information about the low-temperature behavior of the susceptibility, we studied the correlation function $G(M/\sqrt{2})$ defined in (2.1) for various lattice sizes ($M=4$–20). From these results we were able to obtain the correlation length $\xi(T)$ depicted as a function of βJ in Fig. 5. The largest lattices used were $M=16$ and 20. A 16×16 lattice shows significant saturation effects for $\theta\lesssim0.7$ while the 20×20 lattice saturates for $\theta\lesssim0.6$. Hence it is likely that the two points in Fig. 5 at $\beta J>1.4$ do not represent the thermodynamic limit. For $\beta J<1.4$, $\xi(T)$ is well parameterized by the form

$$\xi(T)=r_0\exp(\nu\beta J)\ , \tag{2.9}$$

with $r_0=0.31\pm0.01$ and $\nu=1.91\pm0.06$. It is this expression that we shall use in our finite-size scaling analysis.

Assuming we have an exponent $\eta(T)$ such that

$$\langle s_i^z s_{i+l}^z\rangle\simeq c_0\frac{e^{-|l|/\xi}}{|l|^{\eta}}\ , \tag{2.10}$$

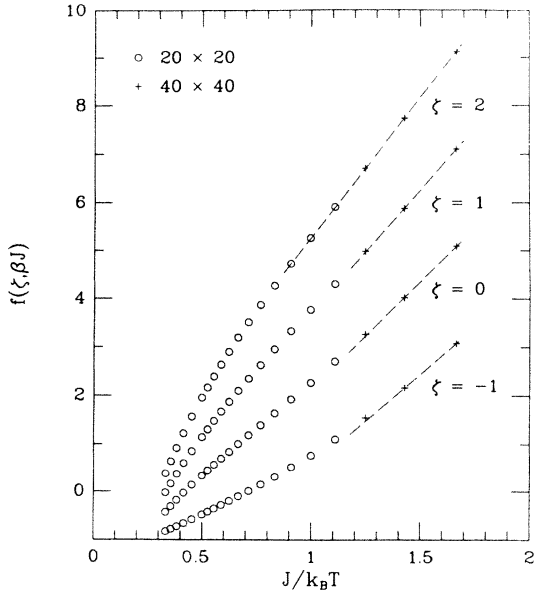

FIG. 4. Plot of $f(\zeta,\beta J)$ as defined in Eq. (2.7) vs βJ for $\zeta=-1$, 0, 1, and 2. The open circles are from the susceptibility of a 20×20 lattice while the crosses are from that of a 40×40 lattice.

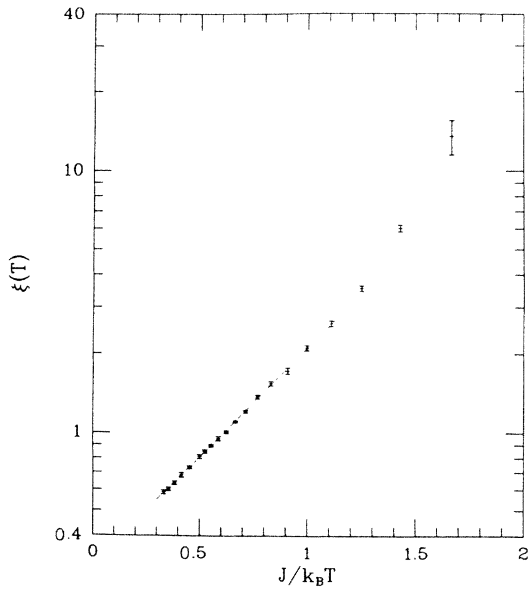

FIG. 5. The correlation length as a function of βJ. The two points at $\beta J>1.4$ are believed to be seriously affected by the finite size of the lattices considered. The line represents the curve $\xi(T)=0.31\exp(1.91\beta J)$.

the susceptibility per site satisfies the finite-size scaling relation

$$\frac{4k_BT\chi}{N(g\mu_B)^2}=\frac{4}{N}\sum_{i,j}\langle s_i^z s_j^z\rangle$$
$$=4c_0\int d^2r\frac{e^{-r/\xi}}{r^\eta}$$
$$=8\pi c_0\xi^{2-\eta}\int_0^{M/\xi}dx\,x^{1-\eta}e^{-x}$$
$$\sim\xi^{2-\eta(T)}F(\xi/M) \tag{2.11}$$
$$\sim M^{2-\eta(T)}\tilde{F}(\xi/M)\,. \tag{2.11'}$$

In the thermodynamic limit, we have

$$\lim_{N\to\infty}\frac{4k_BT\chi}{N(g\mu_B)^2}\sim\xi^{2-\eta(T)}\,. \tag{2.12}$$

If Eq. (2.9) remains valid in the limit $\beta J\to\infty$, Eq. (2.8) leads to the relation

$$\gamma=2\nu\,, \tag{2.13}$$

where we have used the fact that $\eta(T=0)=0$, i.e., the correlations are long ranged at $T=0$. From our analysis of the correlation length [Eq. (2.9)] one would then conclude that $\gamma=3.82\pm0.12$. Going back to Table I, it would appear that ζ is near -1 instead of being 1 or 2 as Fig. 4 would have suggested.

We can get yet more information from the finite-size scaling relation (2.11'). We note that while finite-size scaling is usually applied to a system near its critical point, where η can be treated as a fixed exponent, the η in (2.11') should indeed be a function of the temperature. If the correlation length $\xi(T)$ is not very much larger than M, the saturation effects are still small and Eq. (2.10) remains valid. Under these conditions finite-size scaling will hold, and we may use Eq. (2.11') to estimate the function $\eta(T)$ as per the following procedure. From the knowledge of $\xi(T)$ we may tabulate the various values of $\xi(T)/M$. If we find values (T_1,M_1) and (T_2,M_2) such that

$$\frac{\xi(T_1)}{M_1}=\frac{\xi(T_2)}{M_2} \tag{2.14}$$

to within, say, 2%, we may use the finite-size scaling relation (2.11') to obtain an estimate for $\eta(\bar{T})$ where $\bar{T}$ is an average of T_1 and T_2:

$$\bar{T}=\tfrac{1}{2}(T_1+T_2)\,. \tag{2.15}$$

We have

$$\eta(\bar{T})\simeq 2-\frac{\ln[\Gamma(T_1,M_1)/\Gamma(T_2,M_2)]}{\ln(M_1/M_2)}\,, \tag{2.16}$$

where

$$\Gamma(T,M)\equiv\frac{4k_BT\chi(T,M)}{M^2(g\mu_B)^2}=\frac{4}{M^2}\langle S^zS^z\rangle_{T,M}\,. \tag{2.17}$$

Equation (2.16) becomes quite a good approximation if $\eta(T_1)\simeq\eta(T_2)$ but the factor $[\ln(M_1/M_2)]^{-1}$ amplifies the statistical noise in $\eta(\bar{T})$ due to the $\Gamma(T,M)$ if M_1 is too close to M_2. Hence we use the following restrictions on (T_1,M_1) and (T_2,M_2):

$$\xi/M\le 2\,,$$
$$\left|\ln\left[\frac{M_1}{\xi(T_1)}\frac{\xi(T_2)}{M^2}\right]\right|\le\ln(1.02)\,,$$
$$|T_1-T_2|\le 0.6\,, \tag{2.18}$$
$$\left|\ln\left[\frac{M_1}{M_2}\right]\right|\ge\ln(1.1)\,.$$

Figure 6 is a scatter plot of the various estimates of $\eta(T)$ we have thus obtained. Because of slight mismatches of the ratios in (2.14) and the estimation of the abscissas (2.15), it is very difficult to estimate the uncertainties in these points. One can see, however, that $\eta(T)$ seems to increase approximately linearly with the temperature until it saturates at a value near unity at temperatures greater than $2J$. As $\eta(T)$ should have a temperature dependence of $a\theta-(\zeta+1)\theta\ln\theta$ at low temperatures, the apparent absence of such a logarithmic term is further evidence that $\zeta\simeq-1$.

The author knows of no theoretical predictions for $\eta(T)$. Indeed, even the correlation length $\xi(T)$ has not been well studied in the current literature. Yamaji and Kondo's Green's-function approximation[14] should yield some results on these topics but none are included in Yamaji and Kondo's short paper on the 2D Heisenberg ferromagnet. Our best estimate of the low-temperature behavior of χ is

$$\chi\sim A\frac{N(g\mu_B)^2}{k_BT}\exp(\gamma\beta J)\,, \tag{2.19}$$

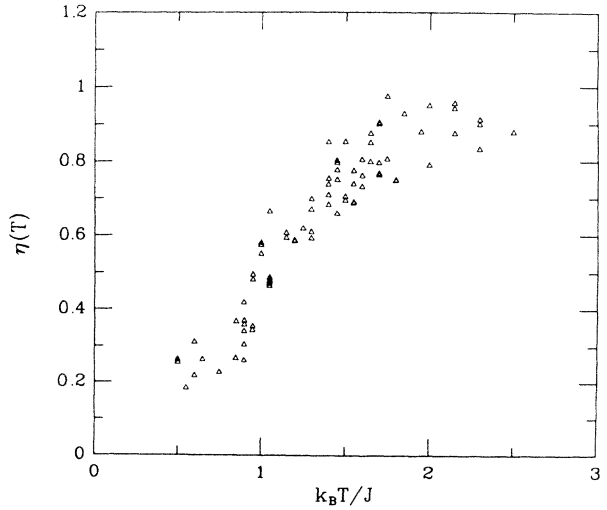

FIG. 6. The exponent $\eta(T)$ vs k_BT/J as determined by applying finite-size scaling as per the procedure in the text [Eq. (2.16)].

where $\gamma=3.82\pm0.12$. The Yamaji-Kondo prediction for the susceptibility [Eq. (1.3)] correctly predicts the T^{-1} prefactor and gives a better value of γ than the Dalton-Wood result [Eq. (1.2)].

III. THE BOND-DILUTED 2D $S=\frac{1}{2}$ HEISENBERG FERROMAGNET

The bond-diluted 2D square lattice has a critical bond concentration of $p_c=0.5$. For $p<p_c$, there does not exist a cluster of infinite size in the thermodynamic limit. Hence there could not be any long-range order. As the 2D Heisenberg ferromagnetic system does not order even for $p=1$ (the full lattice), the behavior near $p=p_c$ cannot be as drastic as that of the dilute 2D Ising model which has a phase transition[28] at $p=p_c$. Nonetheless we can expect a significant increase in the correlation effects and the spin correlation length for $p>p_c$.

Let us consider the spin correlation function of Eq. (2.3):

$$\frac{\chi}{\chi_0}=\frac{4k_BT\chi}{N(g\mu_B)^2}=\frac{4}{N}\langle S^zS^z\rangle\ . \tag{3.1}$$

For a finite lattice this quantity will saturate at some finite value as $T\to0$ for any value of p. The saturation level depends on the sizes of the various clusters and hence will be p dependent. for $p<1$, the interacting spins form separate clusters of size $y_1,y_2,y_3,\ldots,y_l$ where

$$y_1\geq y_2\geq y_3\geq\cdots\geq y_l\ ,$$

and

$$\sum_{i=1}^{l}y_i=N\ . \tag{3.2}$$

Using the same arguments that led to Eq. (2.6), the low-temperature limit of $\langle S^zS^z\rangle$ is given by

$$\lim_{T\to0}\frac{\chi}{\chi_0}=\frac{1}{3N}\sum_{i=1}^{l}y_i(y_i+2)\ . \tag{3.3}$$

To proceed further we need to evaluate the sum in (3.3). For $p\leq p_c$, there is no infinite cluster. We may therefore use the approximation that all the clusters are roughly equal in size:

$$\begin{aligned}&\langle y_i\rangle=y\simeq\frac{N}{\langle l\rangle}\ ,\\&\langle y_i^2\rangle=y^2+\delta^2\ ,\end{aligned} \tag{3.4}$$

where δ^2, the variance of y_i, is expected to be of the order of y. Equation (3.3) then becomes

$$\lim_{T\to0}\frac{\chi}{\chi_0}\simeq\frac{1}{3y}(y^2+2y+\delta^2)\ . \tag{3.5}$$

For $p>p_c$, a finite fraction $f(p)$ of the sites are part of an infinite cluster in the thermodynamic limit. This implies that, for $p>p_c$,

$$y_1=f(p)N\ ,\quad f(p)>0 \tag{3.6}$$

and

$$y_1\gg y_2\geq y_3\geq\cdots\ .$$

The infinite cluster must be handled separately but the derivation of (3.5) still applies to the small (finite) clusters. Equation (3.3) then gives the zero-temperature limit valid for all p:

$$\begin{aligned}&\lim_{T\to0}\frac{4}{N}\langle S^zS^z\rangle\\&\quad\simeq\frac{[1-f(p)]}{3y}(y^2+2y+\delta^2)+\frac{f(p)}{3}[2+f(p)N]\ ,\end{aligned} \tag{3.7}$$

where y is now the average size of the finite clusters. Above p_c, $f(p)>0$ and the second term on the right-hand side of Eq. (3.7) diverges as N in the thermodynamic limit. As $p\to p_c^-$, $f(p)=0$ but y diverges. The mean size of a cluster on an $M\times M$ lattice at $p=p_c$ is given by

$$y=\int d^2r\frac{1}{r^{\eta_c}}\sim M^{2-\eta_c}=N^{1-\eta_c/2}\ , \tag{3.8}$$

where η_c is the value of the exponent η appearing in Eq. (2.10) at $T=0$ and $p=p_c$. This η_c is the same as the exponent η relevant to the pair-connectedness function at $p=p_c$ in the theory of percolation.[6,29] We see that the first term on the right-hand side of Eq. (3.7) will diverge as $N^{1-\eta_c/2}$ in the thermodynamic limit at $p=p_c$. We conclude that, in the thermodynamic limit, χ/χ_0 diverges as $T\to0$ for $p\geq p_c$. For $p<p_c$, χ/χ_0 saturates at a finite value as $T\to0$ in the thermodynamic limit.

Our technique studies the thermodynamics of the bond-diluted systems and is not at all well suited to the study of the percolation exponents which only show up at $T=0$ and for large lattices. However, our simulations can explore the nature of the divergences in $\langle S^zS^z\rangle$ as $T\to0$ for $p\geq p_c$.

To study the thermodynamics of a bond-diluted lattice with a bond probability p, we generated a lattice of size $M\times M$ with each bond being present with the probability p. It is important to study the thermodynamic properties of a particular lattice for the whole range of interesting temperatures as a method of variance reduction. The ensemble average or configurational average is then the average of the thermodynamic properties of several such lattices. Generally we chose to seed the random number generator such that the number of bonds did not differ by more than 2% from the expected number of bonds

$$\langle N_b\rangle=2pN\ . \tag{3.9}$$

All of the results presented here are the average over five lattices for each set of values p, T, and M. For each lattice the simulation typically consisted of ten groups of 1000 observations at each temperature.

As the energy and the specific heat scale with the number of bonds, we have plotted in Fig. 7 the specific heat per bond for the 12×12 lattice at $p=0.25$, 0.5, and 0.75. For $p<1$ the spatial correlation between spins dies away more rapidly, and it appears that for $p\leq0.75$, the 12×12 lattice is already large enough to describe the thermodynamic limit for $\theta\geq0.7$. For comparison we have also included in Fig. 7 the specific heat per bond of the 20×20 $p=1$ lattice. As p decreases from unity, the specific-heat peak occurs at lower temperatures and the peak height decreases from roughly $0.2k_B$ per bond at $p=1$ to about

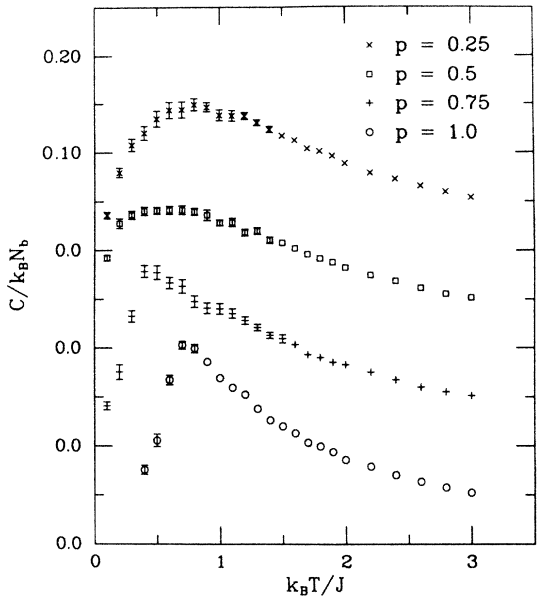

FIG. 7. The specific heat per bond at various bond concentrations. The $p=1$ curve is the specific heat of the full 20×20 lattice, while the curves for $p<1$ are from a study of 12×12 lattices.

$0.14k_B$ per bond at $p=0.5$. At $p=0.5$ the specific heat peak is very broad and it is nearly flat for $0.3\leq\theta\leq1$. At $p=0.25$, we only have small clusters and the specific-heat peak position has shifted back toward the higher temperatures occurring roughly at $\theta=0.8$.

As is to be expected, the magnetic susceptibility shows a much stronger p dependence than the specific heat. Figure 8 depicts the susceptibility per site on a 12×12 lattice at various values of the bond concentration. For $p=1$ and 0.75, the 12×12 lattice has noticeable saturation effects at the lowest temperatures studied. The function plotted is bounded above by $\frac{1}{3}(N+2)$ which is 48.7 for the 12×12 lattice. The susceptibility at $p=0.25$ is saturating at a value much less than this upper bound, a fact consistent with expression (3.7) which says that, for $p<p_c$, the limit

$$\lim_{N\to\infty}\lim_{T\to0}\left[\frac{4k_BT\chi}{N(g\mu_B)^2}\right]$$

exists. The curve at $p=0.5$ seems to be diverging (or reaching saturation) as an inverse power of the temperature as predicted by Stanley *et al.*,[15] Lubensky,[16] and others.[19,20] The behavior at $p=0.5$ will be studied further below. Figure 9 gives the susceptibility as a function of p at the temperature $\theta=0.1$ for three different lattice sizes. At this temperature we see significant saturation effects for all $p\geq0.5$. We immediately note that there is a large increase in the low-temperature susceptibility as p increases through p_c.

For $p_c<p<1$, the dilute lattice still behaves much like the full lattice. Indeed it appears from Fig. 10 that the susceptibility at $p=0.75$ behaves as

$$\frac{4k_BT\chi}{N(g\mu_B)^2}\sim A\exp(\gamma\beta J)\ , \tag{3.10}$$

with

$$\gamma(p=0.75)=1.246\pm0.007\ . \tag{3.11}$$

Furthermore, from Fig. 11, we see that the low-temperature correlation length is well fitted by the expression

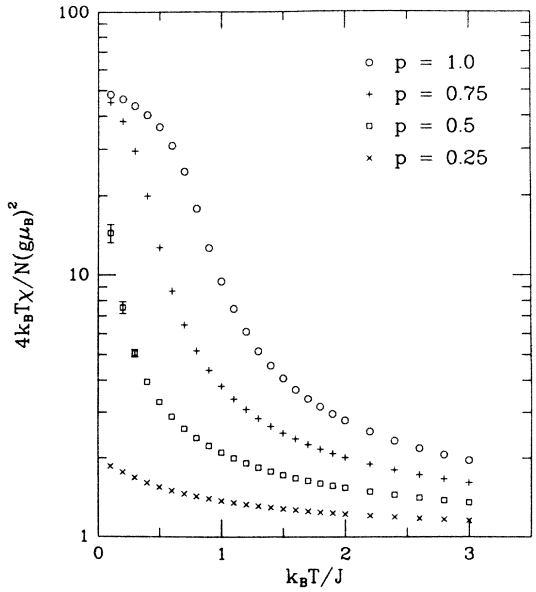

FIG. 8. The magnetic susceptibility per site for the 12×12 lattice at various bond concentrations.

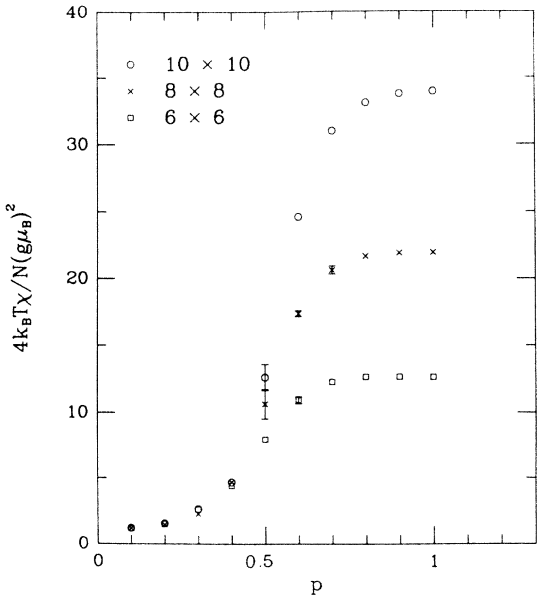

FIG. 9. The magnetic susceptibility per site as a function of the bond concentration p at the temperature $k_BT=0.1J$ for three different lattice sizes.

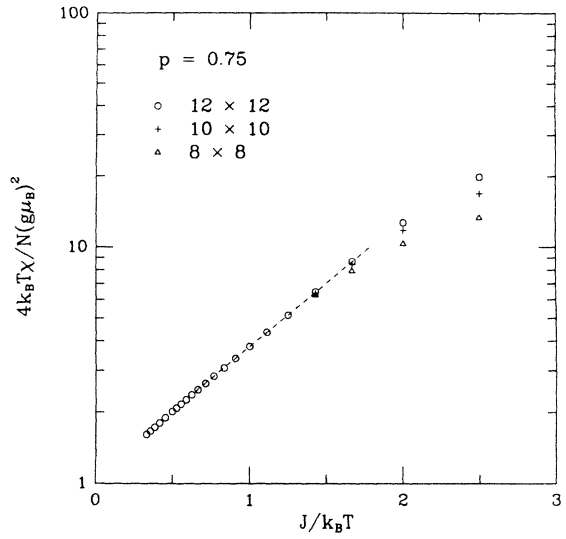

FIG. 10. The magnetic susceptibility per site as a function of the inverse temperature at the bond concentration $p=0.75$. Dashed line corresponds to $1.085e^{1.246\beta J}$.

$$\xi(p,T)=r_0(p)\exp[\nu(p)\beta J]\ , \tag{3.12}$$

with

$$\begin{aligned}&\nu(p=0.75)=0.99\pm0.04\ ,\\ &r_0(p=0.75)=0.396\pm0.025\ .\end{aligned} \tag{3.13}$$

We see that the exponential divergence of χ and ξ is weaker for the bond-diluted lattice than it is for the full lattice where $\nu=1.91\pm0.06$ and $\gamma=2\nu$. Rewriting the scaling relation (2.12) as

$$\gamma=\nu(2-\eta)\ , \tag{3.14}$$

a comparison of Eqs. (3.11) and (3.13) indicates that, contrary to the full lattice result, we have

$$\eta(p=0.75,T=0)\neq0\ ,$$

but instead it appears that

$$\eta(p=0.75,T=0)\simeq0.74\pm0.05\ . \tag{3.15}$$

Even at $T=0$, the correlations are not long ranged when $p<1$. In the bond-diluted lattice some sites are totally uncorrelated with the rest of the lattice.

We now turn our attention to $p=p_c$ to study the thermodynamic behavior near the percolation threshold. Figure 12 is a log-log plot of the susceptibility versus the temperature for the 12×12 lattice at the bond concentration $p=p_c=0.5$. The low-temperature susceptibility appears to behave as [see Eq. (1.6)]

$$T\chi(p=p_c,T)\sim\theta^{-\gamma_T}\ , \tag{3.16}$$

where

$$\gamma_T\simeq0.95\pm0.08\ . \tag{3.17}$$

For comparison, the 10×10 lattice gives $\gamma_T\simeq0.86\pm0.18$ and for the 8×8 lattice $\gamma_T\simeq0.77\pm0.04$. These values of γ_T were obtained by neglecting the lowest-temperature values where the saturation effects are apparent. The finite-size dependence of our γ_T values suggests that (3.17) is not yet characteristic of the thermodynamic limit.

By studying lattices of size ranging from 4×4 to 12×12 we obtained estimates of the correlation length

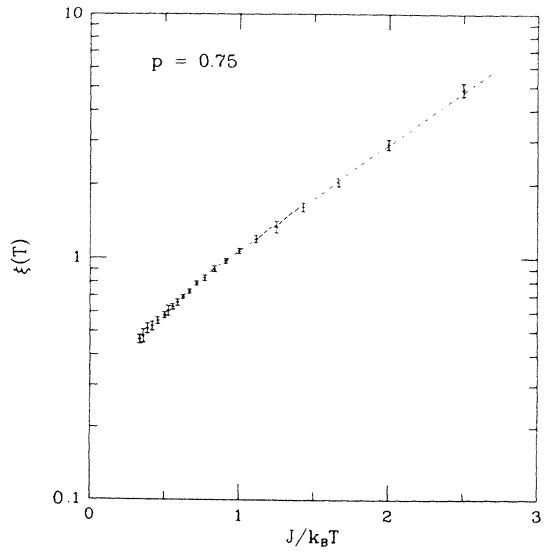

FIG. 11. The correlation length as a function of the inverse temperature for the bond concentration $p=0.75$. Dashed line corresponds to $\xi=0.396e^{0.99\beta J}$.

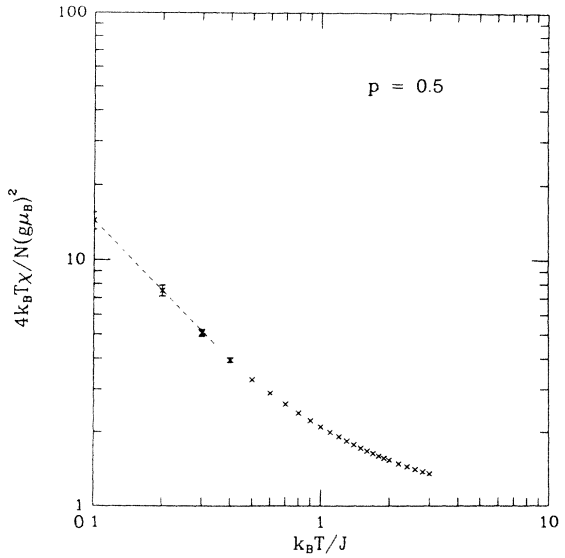

FIG. 12. The magnetic susceptibility per site vs the temperature for the 12×12 lattice at the bond concentration $p=p_c=0.5$. Dashed line corresponds to $1.67\theta^{-0.95}$.

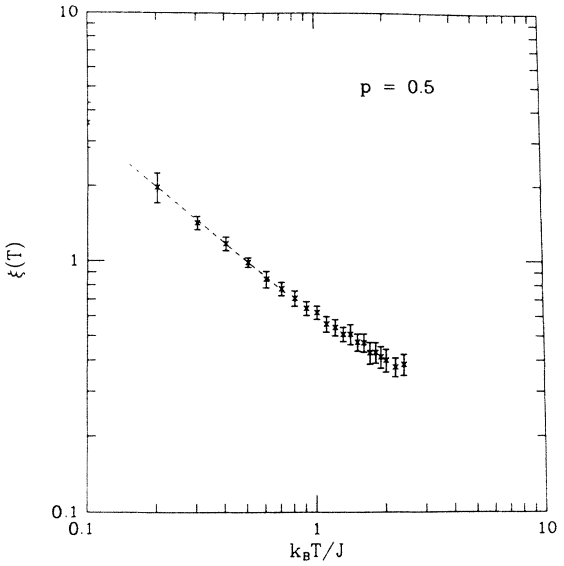

FIG. 13. The correlation length vs the temperature at the bond concentration $p=p_c=0.5$. Dashed line corresponds to $\xi=0.581\theta^{-0.76}$.

$\xi(p=p_c,T)$. These estimates are plotted in Fig. 13, and we see that the low-temperature correlation length does behave as an inverse power of the temperature [see Eq. (1.6)]:

$$\xi(p=p_c,T)\sim\theta^{-\nu_T}\ , \tag{3.18}$$

where

$$\nu_T=0.76\pm0.05 \tag{3.19}$$

The above results are to be compared to the experimental values obtained by Birgeneau *et al.*[30] for the 2D $S=\frac{5}{2}$ Heisenberg antiferromagnet:

$$\nu_T=0.9\pm0.1\ ,\quad \gamma_T=1.5\pm0.15\ , \tag{3.20}$$

and the renormalization-group predictions[20] for the classical 2D HF:

$$\nu_T=0.93\ ,\quad \gamma_T=1.7\ . \tag{3.21}$$

Our value for γ_T [Eq. (3.17)] is definitely lower than these other values. However, our value of ν_T [Eq. (3.19)] is not so far from the experimental value of Birgeneau *et al.* when the uncertainties in the two values are considered.

Further studies of the bond-diluted lattice are in progress on lattices larger than 12×12 in order to study the thermodynamic limit at the lower temperatures with particular emphasis on the percolation limit $p=p_c$.

ACKNOWLEDGMENTS

The author would like to thank Professor D. J. Scalapino for many helpful suggestions and comments. The author also benefited from ideas inspired by a copy of a program kindly sent to him by S. Chakravarty. The author would like to acknowledge financial support of the Natural Sciences and Engineering Research Council of Canada. This work was also supported in part by the National Science Foundation under Grant No. DMR83-20481.

APPENDIX

We present here a full description of the Monte Carlo algorithm including some technical details we used to speed up the algorithm. We also comment on the performance of the algorithm and we discuss why the method fails when we try to use it with an antiferromagnetic coupling.

It is clear that the simulation outlined in the Introduction can be implemented if there exists some simple and efficient method of calculating the traces involved in Eqs. (1.12) and (1.16). It is here that we use the fact that $\hat{C}_n$, being a product of permutations, is also a permutation operator. Upon factoring $\hat{C}_n$ into a product of disjoint cycles, one readily sees that

$$\mathrm{Tr}(\hat{C}_n)=2^{k(C_n)}\ , \tag{A1}$$

where $k(C_n)$ is the total number of cycles in the permutation $\hat{C}_n$ including the trivial cycles of length one. One also finds that

$$\frac{4\,\mathrm{Tr}(\hat{C}_n s_i^z s_j^z)}{\mathrm{Tr}(\hat{C}_n)}=\begin{cases}1 & \text{if sites } i \text{ and } j \text{ are part of the same cycle}\\ 0 & \text{otherwise}\end{cases} \tag{A2}$$

or two spins are uncorrelated unless they belong to the same cycle. Equations (A1) and (A2) allow us to perform the simulation and measure the susceptibility and the correlation length. We note that any contribution to $4\langle s_i^z s_j^z\rangle$ is either 0 or 1. Measuring a correlation of order 10^{-5} will therefore necessitate several times 10^5 observations. This technique is clearly not suitable for measuring very small correlations. Using Eqs. (1.15), (1.16), (A2), and the fact that $\langle S^z\rangle=0$ in 2D, the susceptibility is given by

$$\frac{4k_BT\chi}{(g\mu_B)^2}=4\sum_{i,j}\langle s_i^z s_j^z\rangle =\left\langle\sum_{j=1}^{k(C_n)}a_j^2\right\rangle_\Pi\ , \tag{A3}$$

where a_j is the length of the jth cycle of the permutation $\hat{C}_n$ and the $\langle\ \rangle_\Pi$ denotes an average with respect to the probability distribution $\Pi(C_n)/Z$.

Lyklema[23] and Chakravarty and Stein[24] proposed that the energy and the specific heat be measured using the expressions

$$E=\langle\hat{H}\rangle=-k_BT\langle n\rangle_\Pi+JN_b/2\ , \tag{A4}$$

and

$$C=k_B(\langle n^2\rangle_\Pi-\langle n\rangle_\Pi^2-\langle n\rangle_\Pi)\ . \tag{A5}$$

We found that the statistical properties of the measurements were improved if we used the estimator

$$X(C_n)\equiv\sum_{i=1}^{N_b}\frac{\mathrm{Tr}(\hat{P}_i\hat{C}_n)}{\mathrm{Tr}(\hat{C}_n)}\ . \tag{A6}$$

With this estimator we have the alternative expressions for the energy and the specific heat:

$$E=-J\langle X\rangle_\Pi+JN_b/2\ , \tag{A7}$$

and

$$C=k_B\beta J(\langle nX\rangle_\Pi-\langle n\rangle_\Pi\langle X\rangle_\Pi)\ . \tag{A8}$$

To perform the Monte Carlo random walk among the sequences C_n, we set up a Markov chain with the limiting distribution $\Pi(C_n)$. We proceed along the lines of Handscomb's original proposal.[25] We only consider moves which change the length of the sequence n by one: a forward move corresponding to the addition of the one bond at the end of the sequence or a backward move corresponding to the deletion of the first bond in the sequence. The forward move is attempted with the probability

$$f(n)=\frac{\max(n+1,2)}{2(n+1)} \tag{A9}$$

and we choose the bond to be inserted at random from the N_b bonds in the Hamiltonian. A forward move $C_n\rightarrow C_{n+1}=C_ni$ is accepted with the probability

$$\begin{aligned}\alpha_{C_n,C_ni}&=\min\left\{1,\frac{1-f(n+1)}{f(n)/N_b}\frac{\Pi(C_ni)}{\Pi(C_n)}\right\}\\&=\min\left\{1,\frac{\beta JN_b}{\max(n+1,2)}\frac{\mathrm{Tr}(\hat{P}_i\hat{C}_n)}{\mathrm{Tr}(\hat{C}_n)}\right\},\end{aligned} \tag{A10}$$

while the acceptance probability for a backward move $C_n=i_1C_{n-1}\rightarrow C_{n-1}$ may be written as

$$\alpha_{i_1C_{n-1},C_{n-1}}=\min\left\{1,\frac{\max(n,2)}{\beta JN_b}\frac{\mathrm{Tr}(\hat{P}_{i_1}\hat{C}_n)}{\mathrm{Tr}(\hat{C}_n)}\right\}. \tag{A11}$$

In the event a backward move is rejected, we rotate the sequence by one bond

$$i_1C_{n-1}\rightarrow C_{n-1}i_1\ . \tag{A12}$$

The acceptance probabilities (A10) and (A11) correspond very closely to the usual Metropolis algorithm,[31] the main difference being that in a true Metropolis algorithm each move is reversible.

In contrast to the work of Lyklema[23] and Chakravarty and Stein,[24] one should not rotate the sequence by a random amount after a backward move is rejected. For Handscomb's proof that $\Pi(C_n)$ is the limiting distribution of the Markov chain to be valid, we need to use the single-bond rotation described by (A12). One can use rotations by a random amount as long as such rotations do not depend on the rejection or acceptance of any move. Indeed we rotated the sequence by a random amount after each observation.

To get the ratio of the traces in (A10) and (A11) one does not need to count the cycles in $\hat{P}_i\hat{C}_n$ as suggested by (A1). One simply needs to know if the sites k and l involved in the bond $\hat{P}_i$ are already in the same cycle in $\hat{C}_n$. We have

$$\frac{\mathrm{Tr}(\hat{P}_i\hat{C}_n)}{\mathrm{Tr}(\hat{C}_n)}=\begin{cases}2 & \text{if } k,l \text{ are in the same cycle in } C_n\\ \frac{1}{2} & \text{if } k,l \text{ are not in the same cycle}\ .\end{cases} \tag{A13}$$

This determination can be evaluated very quickly by keeping an up-to-date evaluation of the permutation $\hat{C}_n$ at all times. Similarly, we use Eq. (A13) while evaluating the observable $X(C_n)$ defined in (A6). This concludes our description of the algorithm, and we shall now present a discussion of the performance of this technique.

At low temperatures,[32] we have the approximate expectation value

$$\langle n\rangle_\Pi\simeq\beta JN_b[1+O(\beta J)^{-x-1}]\ , \tag{A14}$$

where x is some positive exponent ($x=\frac{1}{2}$ for the 1D Heisenberg model).[18] Hence the length of the sequences of interest grows linearly with βJ. As the specific heat remains finite and indeed goes to zero as $\beta J\rightarrow\infty$, Eq. (A5) implies that

$$\langle n^2\rangle_\Pi-\langle n\rangle_\Pi^2\simeq\langle n\rangle_\Pi\ . \tag{A15}$$

At low temperatures the distribution of n then becomes very nearly a Poisson distribution with mean

$$\lambda=\beta JN_bz\ , \tag{A16}$$

where $z\simeq1$. This approximate Poisson distribution allows us to make certain statements about the behavior of the simulation in the low-temperature limit.

We first use this approximate Poisson distribution to discuss the antiferromagnetic case ($J<0$). Instead of Eqs. (1.11) and (1.15), we would have in the antiferromagnetic case

$$Z_{\mathrm{AF}}=\sum_n\sum_{C_n}(-1)^n\Pi(C_n)\ , \tag{A17}$$

and

$$\begin{aligned}\langle\hat{A}\rangle&=\frac{1}{Z_{\mathrm{AF}}}\sum_n\sum_{C_n}\Pi(C_n)(-1)^n\frac{\mathrm{Tr}(\hat{C}_n\hat{A})}{\mathrm{Tr}(\hat{C}_n)}\\&=\frac{\langle(-1)^n\Omega_A(C_n)\rangle_\Pi}{\langle(-1)^n\rangle_\Pi}\ ,\end{aligned} \tag{A18}$$

where $\Pi(C_n)$ is the same distribution as for $J>0$ and can therefore be approximated by the Poisson distribution for large $|\beta J|$. A straightforward calculation then yields

$$\langle(-1)^n\rangle_\Pi\simeq e^{-2\lambda}=e^{-2\beta JN_bz}\ . \tag{A19}$$

The normalization factor $\langle(-1)^n\rangle_\Pi$ for all observables goes to zero *exponentially* with the product of $|\beta J|$ and the number of bonds. Statistical fluctuations will there-

fore become very important even for moderate $|\beta J|$ if N_b becomes large.[32] Hence a naive implementation of this Monte Carlo technique is simply not appropriate to the antiferromagnetic Heisenberg problem. Other techniques[24,26] must be used.

One can also use the approximate Poisson distribution to estimate the relaxation time in our Monte Carlo simulation. With this distribution we have the approximate equation of motion ($\lambda \gg 1$)

$$\frac{\partial n}{\partial t}(t) \simeq -\frac{(n-\lambda)}{2\lambda} . \tag{A20}$$

It follows that

$$\langle n(t)n(0)\rangle - \langle n\rangle^2 \simeq \lambda e^{-t/2\lambda} . \tag{A21}$$

The relaxation time is

$$\tau = 2\lambda = 2\beta J N_b z \simeq 2\beta J N_b , \tag{A22}$$

or it takes roughly 2λ steps in the random walk for the sequence to lose its memory, at least as far as the observable n is concerned. Because of these correlations, there is no point in making an observation after every step in the random walk.[33] If one makes an observation after every m steps, m should be of the order of λ or $\beta J N_b$ for maximum efficiency. In our simulations we usually used m equal to the number of lattice sites N. With N_b given by

$$N_b = pdN = 2pN , \tag{A23}$$

where p is the bond probability, the relaxation time measured in observations is then

$$\tau = 4p\beta J . \tag{A24}$$

We usually allowed a time of 50 or 100 observations to reach equilibrium before taking measurements.

By not taking measurements too often, the speed of the simulation is essentially determined by the speed with which one can evaluate the ratio (A13) for the successive random walk steps. At lower temperatures and for larger lattices the typical cycle length grows [see, for example, Eqs. (1.3) and (A3)], and it takes longer to determine whether two sites k and l belong to the same cycle or not. Most of the simulations were done on a Texas Instruments TI-99/4A microcomputer programmed in assembly language. The typical time needed per possible step ranged from about 1.5 msec at $\theta \gtrsim 1$ (any lattice) to 2.4 msec (6×6 lattice) and 6.0 msec (20×20 lattice) at $\theta = 0.3$. This corresponds to roughly 12—20 observations per second for a 6×6 lattice and 0.42—1.7 observations per second for the 20×20 lattice. The same program written in FORTRAN on a Digital Equipment Corporation VAX 750 was only about 2.5 times faster. The dedicated TI-99/4A was therefore faster and much more economical than the time-shared VAX 750. Of course, this is so because the simulation uses almost only integer arithmetic.

The largest lattice that can be studied by the TI-99/4A computer is 22×22. Furthermore, we are restricted to temperatures such that $\beta J N_b \lesssim 4500$. The 40×40 lattice result in Fig. 3 was obtained on a VAX 750 which is not so limited by memory. On a large lattice even a short run gives quite good relative precision in the measurements of the macroscopic observables.

One final note concerns the measurement of the specific heat. From Eq. (A8) we see that for a specific heat behaving as

$$C \sim N_b \theta^x$$

in the low-temperature limit, we need to subtract two terms of order $\beta J N_b^2$ to obtain a residual of order $N_b/(\beta J)^{x+1}$. We would need to know $\langle nX\rangle_\Pi$ to a relative precision of roughly $[N_b(\beta J)^{x+2}]^{-1}$. For this reason it becomes impractical to measure the specific heat directly at low temperatures. We instead get the low-temperature specific heat by differentiating the energy with respect to the temperature as it is quite easy to get very good relative precision for the energy at any temperature.

*Permanent address: Department of Physics, University of Delaware, Newark, DE 19716.

[1]N. D. Mermin, J. Math. Phys. **8**, 1061 (1967).
[2]D. S. Fisher and D. R. Nelson, Phys. Rev. B **16**, 2300 (1977).
[3]J. L. Cardy and H. W. Hamber, Phys. Rev. Lett. **45**, 499 (1980).
[4]P. Bloembergen, Physica **85B**, 51 (1977).
[5]I. Yamada, I. Morishita, and T. Tokuyama, Physica **115B**, 179 (1983).
[6]See, for example, the review by J. W. Essam, Rep. Prog. Phys. **43**, 833 (1980).
[7]R. J. Elliot, J. A. Krumhansl, and P. L. Leath, Rev. Mod. Phys. **46**, 465 (1974), and references therein; T. Odagaki and M. Lax, Phys. Rev. B **24**, 5284 (1981); I. Webman, Phys. Rev. Lett. **47**, 1496 (1981); Kin-Wah Yu, Phys. Rev. B **29**, 4065 (1984).
[8]M. F. Sykes and J. W. Essam, J. Math. Phys. **5**, 1117 (1964).
[9]M. F. Sykes, D. S. Gaunt, and M. Glen, J. Phys. A **9**, 97 (1976).
[10]G. A. Baker, Jr., H. E. Gilbert, J. Eve, and G. S. Rushbrooke, Phys. Lett. **25A**, 207 (1967).
[11]R. Navarro and L. J. de Jongh, Physica **84B**, 229 (1976).
[12]K. Yamaji and J. Kondo, J. Phys. Soc. Jpn. **35**, 25 (1973).
[13]N. W. Dalton and D. W. Wood, Proc. Phys. Soc., London **90**, 459 (1967).
[14]K. Yamaji and J. Kondo, Phys. Lett. **45A**, 317 (1973); J. Kondo and K. Yamaji, Prog. Theor. Phys. **47**, 807 (1972).
[15]H. E. Stanley, R. J. Birgeneau, P. J. Reynolds, and J. F. Nicoll, J. Phys. C **9**, L553 (1976).
[16]T. C. Lubensky, Phys. Rev. B **15**, 311 (1977).
[17]H. E. Stanley, Phys. Rev. **179**, 570 (1969).
[18]J. C. Bonner and M. E. Fisher, Phys. Rev. **135**, A640 (1964).
[19]R. B. Stinchcombe, J. Phys. C **12**, 4533 (1979).
[20]A. Coniglio, Phys. Rev. Lett. **46**, 250 (1981); J. Phys. A **15**, 3829 (1982).
[21]D. J. Scalapino and R. L. Sugar, Phys. Rev. Lett. **46**, 519 (1981); R. Blankenbecler, D. J. Scalapino, and R. L. Sugar, Phys. Rev. D **24**, 2278 (1981); E. Loh, Jr., D. J. Scalapino, and P. M. Grant, Phys. Rev. B **31**, 4712 (1985); H. De Raedt and A. Lagendijk, Phys. Rev. Lett. **46**, 77 (1981); H. De Raedt, B. De Raedt, J. Fivez, and A. Lagendijk, Phys. Lett. **104A**, 430 (1984); J. J. Cullen and D. P. Landau, Phys. Rev. B

27, 297 (1983).
[22]G. Parisi and Wu Yongshi, Sci. Sin. **24**, 483 (1981); G. Parisi, Nucl. Phys. **B180**, 378 (1981).
[23]J. W. Lyklema, Phys. Rev. Lett. **49**, 88 (1982).
[24]S. Chakravarty and D. B. Stein, Phys. Rev. Lett. **49**, 582 (1982).
[25]D. C. Handscomb, Proc. Cambridge Philos. Soc. **58**, 594 (1962); **60**, 115 (1964).
[26]D. H. Lee, J. D. Joannopoulos, and J. W. Negele, Phys. Rev. B **30**, 1599 (1984).
[27]Bonner and Fischer (Ref. 18) used a different argument to obtain the same result for the Heisenberg ferromagnetic chain. Their argument remains valid in the two-dimensional case.
[28]See, for example, T. Kaneyoshi, I. Tamura, and R. Honmura, Phys. Rev. B **29**, 2769 (1984), and references therein.
[29]Appendix 1 of Ref. 6 lists $n_c \simeq 0.19$ in two dimensions.
[30]R. J. Birgeneau, R. A. Cowley, G. Shirane, J. A. Tarvin, and G. H. Guggenheim, Phys. Rev. B **21**, 317 (1981).
[31]W. K. Hastings, Biometrika **57**, 97 (1970).
[32]At high temperatures, the spins become totally uncorrelated so that Eq. (1.1) gives $\langle \hat{H} \rangle \to 0$ as $\beta J \to 0$. Alternatively, we see from Eq. (1.10) that $\langle \hat{H} \rangle \to -JN_b/2$ as $T \to 0$. Hence (A4) gives us the inequalities $\beta J N_b/2 \leq \langle n \rangle_\Pi \leq \beta J N_b$.
[33]K. Binder, J. Magn. Magn. Mater. **15-18**, 210 (1980).